Composite Structures 209 (2019) 490–498

Contents lists available at ScienceDirect

Composite Structures

journal homepage: www.elsevier.com/locate/compstruct

Cryogenic and high temperature compressive properties of Metal Foam Matrix Composites

Emanoil Linul[a,*], Liviu Marşavina[a], Petrică-Andrei Linul[b,c], Jaroslav Kovacik[d]

[a] Department of Mechanics and Strength of Materials, Politehnica University of Timisoara, 1 Mihai Viteazu Avenue, 300 222 Timisoara, Romania
[b] Faculty of Industrial Chemistry and Environmental Engineering, Politehnica University of Timisoara, 6 Vasile Parvan Blvd., 300 223 Timisoara, Romania
[c] National Institute of Research for Electrochemistry and Condensed Matter, Aurel Paunescu Podeanu Street 144, 300 569 Timisoara, Romania
[d] Institute of Materials and Machine Mechanics, Slovak Academy of Sciences, Dúbravská cesta 9, 845 13 Bratislava, Slovak Republic

ARTICLE INFO

Keywords:
Cryogenic and elevated temperature
Closed-cell aluminum alloy foams
Metal foam matrix composites
Compressive mechanical properties
Energy absorption capability

ABSTRACT

The cryogenic (−196 °C), room (25 °C) and high (250 °C) temperature compressive crushing performances of recently developed metal foam matrix composites was investigated with respect to the position of reinforcements on foam samples. Closed-cell aluminum alloy foams were produced via powder metallurgical route from AlSi10 matrix material; while diamond shape expanded stainless steel were used as reinforcements. The deformation behavior and main mechanical properties of the unreinforced and reinforced metallic foam was found to be strongly temperature dependent under quasi-static loading. Reinforced foams exhibited much higher strength properties and energy absorption capability compared to unreinforced foams at almost the same overall weight of the samples, i.e. up to 11 times. The properties percentage reductions of the reinforced foams are significantly below the reduction of the unreinforced foam. Furthermore, it was observed that the collapse mechanisms and mechanical properties of the reinforced foams depends on reinforcement position.

1. Introduction

Conventional Composite Metal Foams (CMFs) [1–4] and recently developed Metal Matrix Syntactic Foams (MMSFs) [5–9] are a new class of advanced composite cellular materials of great interest that can be found in every field of today's engineering world. Their particular porous structure gives them unique mechanical and physical properties that allow a broadening in the range of properties of their solid counterparts [10–12]. The applications of these foamed closed-cell porous materials in advanced composite structures (ACSs) are thus very extensive, while the use of fully dense solid materials have lost slowly their applicability [13–15]. Due to its outstanding energy absorption capabilities, high stiffness-to-weight ratio, good fracture and shear strength and exceptional heat transfer ability, they are of special interest in construction, automotive and aeronautics industries [16–19].

Different lightweight and less expensive ACSs capable of low and high temperature operation are also required for many future space exploration missions (and not only). Some typical cold and hot environmental temperatures, applicable for our Solar System, are: the chilly night side of the Mercury (−180 °C), Moon Titan surface temperature (−180 °C), Moon Europa Icy surface temperature (−188 to −143 °C), Saturn cloud tops mean temperature (−185 °C), Uranus (−195 °C) and Neptune (−200 °C) mean temperatures, Venus atmosphere (150 °C between 40 and 48 km altitude and 325 °C at 18 km altitude), the day side of the Mercury (from 150 °C up to 427 °C with an average of 167 °C), on Venus (from −173 °C to 467 °C) etc. [20,21].

Over the past few decades, extensive studies have been performed exploring porous materials suitability for Earth living conditions applications [22–24], while a very limited number of studies have focused on space extreme exploration conditions [25–27]. Even so, the vast majority of these studies were conducted for closed-cell polymeric foams and open-cell metallic foams (MFs) regarding their thermal performances [28–30]. The main cryogenic characteristics of chopped fiber reinforced polyurethane foams [31,32], polymeric foams [33] and sandwich-type insulation board composed of E-glass/epoxy composite and polymeric foams [34] are reported in the literature under both static and impact loading conditions. Fesmire and co-workers [35] have studied the cryogenic thermal performance of Spray-on foam insulation (SOFI) under large temperature differentials. The authors also address recent advancements and applications of SOFI systems on future launch vehicles and spacecraft. More recently, Dixit and Ghosh [36,37] and Chunhui and co-workers [38] have investigated the thermal conductivity of high porosity open-cell MFs as advanced thermal storage unit at low temperatures. The results show that the thermal

* Corresponding author.
E-mail address: emanoil.linul@upt.ro (E. Linul).

https://doi.org/10.1016/j.compstruct.2018.11.006
Received 15 October 2018; Received in revised form 29 October 2018; Accepted 2 November 2018
Available online 03 November 2018
0263-8223/

Nomenclature

ACSs	advanced composite structures
AFs	aluminum foams
b	thickness of reinforcement
CMFs	composite metal foams
CT	cryogenic temperature
EDM	electric discharge machining
E_{qe}	quasi-elastic modulus
h	width of reinforcement
HT	high temperature
H_1	large diagonal of the reinforcement unit-cell
H_2	small diagonal of the reinforcement unit-cell
LR	longitudinal reinforced
MFs	metallic foams
MFMCs	metal foam matrix composites
MMSFs	metal matrix syntactic foams
OSD	onset strain of densification
PM	powder metallurgical route
RT	room temperature
SOFI	spray-on foam insulation
SSFES	stainless steel flat expanded sheets
TR	transversal reinforced
UR	unreinforced
W	energy absorption
W_D	energy absorption at densification strain
α	angle that defines the loading direction
$\Delta\sigma$	stress drop
ε	compressive strain
ε_D	densification strain
ε_y	strain corresponding to compressive yield stress
σ	compressive stress
σ_d	densification stress
σ_{pl}	plateau stress
σ_y	compressive yield stress
$\sigma_{20\%}$	compressive strength at 20%
$\sigma_{40\%}$	compressive strength at 40%

conductivity increases with the temperature decreasing [38]. In addition, Dixit and Ghosh [36] have noticed that between copper and aluminum foam of same weight, copper foam cools down faster. Moreover, Dixit and Ghosh [37], found a decrease in volumetric flow rate of convective fluid indicating lesser heat load results in reduction of foam temperature.

Similarly, the favorable physical and mechanical properties of different porous materials at low temperatures are mentioned in other sources [39–43], but the reported experimental results are not for reinforced closed-cell aluminum foams. The cryogenic and elevated temperature reliability of the MFs is a remaining concern in the space explorations since MFs are subjected to various thermal/mechanical loads due to the temperature difference between the extreme atmospheric space conditions and the weight of the spacecraft components. In practice, the effects of low and high temperatures, on the composites mechanical behavior, can't be ignored because porous (foam) materials are very sensitive to temperature changes [44–46]. Therefore, understanding the mechanical behavior of such cellular materials under extreme atmospheric conditions (from cryogenic to high temperatures) is very important and critical for exploring their suitability for constructing lightweight foam composite structures used in space explorations and Earth living conditions.

To the best of the author's knowledge, the effect of low and high temperatures on the compressive performances of Metal Foam Matrix Composites (MFMCs), particularly with very thin stainless steel mesh reinforcements (~0.5 mm), is not investigated. Therefore, the objective of this work is to present results illustrating the effect of systematic variations of temperature (−196, 25 and 250 °C) and sample configuration (without reinforcements and with two different positioning of reinforcements) on the quasi-static compressive mechanical response of closed-cell aluminum alloy foams.

2. Experimental program

2.1. Materials

Three different types of panels (geometry 30 mm × 500 mm × 500 mm) were manufactured, as follow: unreinforced (UR), transversal reinforced (TR) and longitudinal reinforced (LR) aluminum foams (AFs) panels. The closed-cell aluminum alloy foams investigated in this research were prepared by powder metallurgical (PM) route from AlSi10 matrix composition (10 wt% Si and Al balanced), using 0.4 wt% of TiH_2 as a foaming agent. Composite TR and LR panels with high porosity were reinforced at two loading surfaces with Stainless Steel Flat Expanded Sheets (SSFES). The SSFES reinforcements (square weight of 3.4 kg/m^2) had a diamond shape (H_1 = 6 mm × H_2 = 3 mm), with thickness of b = 0.5 mm and a width of h = 1 mm. Fig. 1 present the geometrical parameters of a SSFES unit-cell

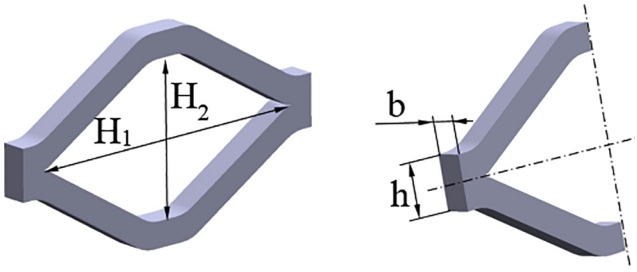

Fig. 1. Geometrical parameters of the SSFES unit-cell.

The used X5CrNi 18–10 stainless steel composition of the SSFES is Cr 17–19.5%, Ni 8–10.5, C < 0.07%. It is austenitic Cr-Ni stainless steel with corrosion resistance to most oxidizing acids and salt spray [47]. The SSFES reinforcements are inserted into the mold together with foamable precursors. During foam expansion, the properly positioned SSFES are infiltrated with molten material thus forming a strong metallurgical bond (due to the reaction between the liquid foam alloy and reinforcements), see Fig. 2a. The quality of the AFs-SSFES bond depends on the chemical composition of both foam and reinforcement materials. If necessary, this bond can be controlled/improved by both coating processes and proper surface treatment of the reinforcements. Besides increasing the foam mechanical properties, the reinforcements prevent liquid foam from collapsing on cooling showing an additional stabilizing effect, thus allowing higher final porosity of the foam [48].

In order to prevent any damage to the foam cellular structure (Fig. 2c), an Electric Discharge Machining (EDM) was used for cutting samples. Therefore, cubes samples (geometry 30 mm × 30 mm × 30 mm), with an average density of 0.42 g/cm^3 were cut from large produced panels (Fig. 2b). The samples with density above or below the 10% range were excluded prior experiments.

2.2. Test set-up

Quasi-static uniaxial compression tests were carried out on a 100 kN A009 (LBG TC100) Universal testing machine equipped with both a cryogenic installation (for low temperature) and a thermal chamber (for high temperature). Therefore, the experimental program it was

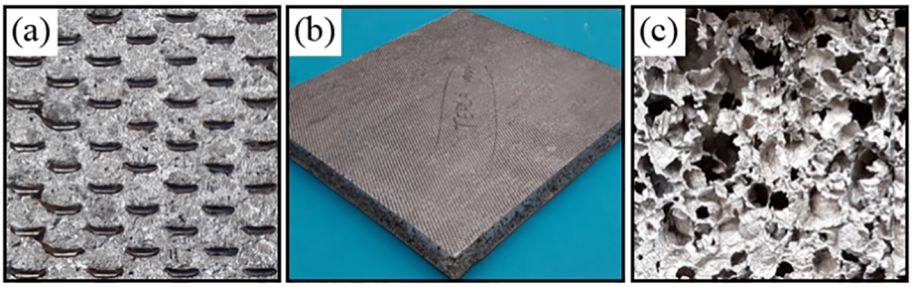

Fig. 2. The infiltrated SSFES cells (a), foamed panel (b) and AFs structure (c).

designed for three different testing temperatures, i.e. −196 °C (cryogenic temperature tests – CT), 25 °C (room temperature tests – RT) and 250 °C (high temperature tests – HT). The experimental tests were performed on cubic samples with three different configurations (UR, TR and LR). The name of the TR and LR are given by the loading direction developed on the reinforcement cells. Therefore, the reinforced foam samples were tested under two different cell directions of α = 0° or TR (Fig. 3a) and α = 90° or LR (Fig. 3b). Fig. 3 illustrates the SSFES orientation along with the loading direction. The low temperature sample tests are performed submerged in liquid nitrogen.

According to the ISO13314-11 standard [49], for test condition, three tests were conducted in order to check the repeatability of the results and a constant crosshead speed of 10 mm/min was used. The experimental test set-up was designed in such a way that the all samples reached a homogenous temperature distribution prior to quasi-static compression. Therefore, all samples were precooled (−196 °C)/preheated (250 °C) in the cryogenic/thermal chamber for 20 min. In order to prevent any reduction in temperature after precooling/preheating, the foam samples were compressed inside the cryogenic/thermal chamber.

3. Results

Based on the load–displacement data recorded by the acquisition system and software of the testing machine, the engineering stress (σ) – engineering strain (ε) graphs were obtained. Figs. 4 and 5 shows the influence of reinforcements (UR, TR and LR) and influence of testing temperature (−196, 25 and 250 °C) on the quasi-static compressive

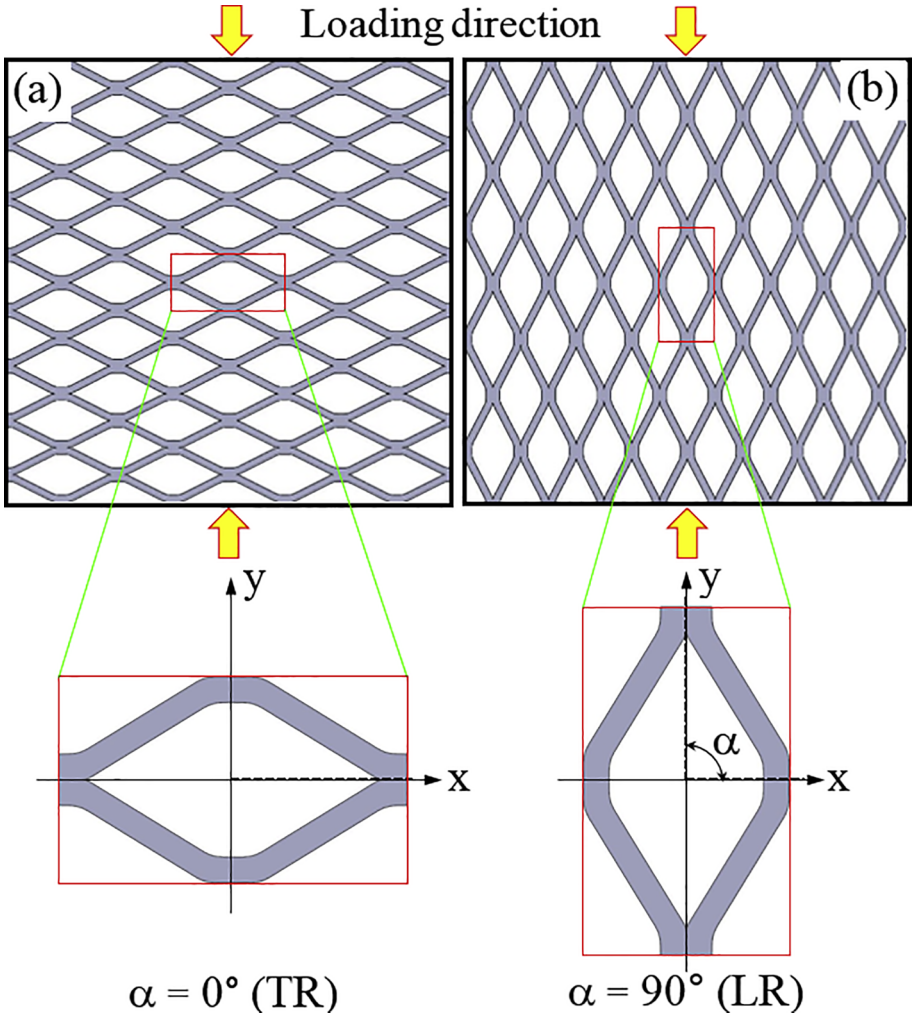

Fig. 3. Orientation of SSFES cells and pattern close-up according to loading directions.

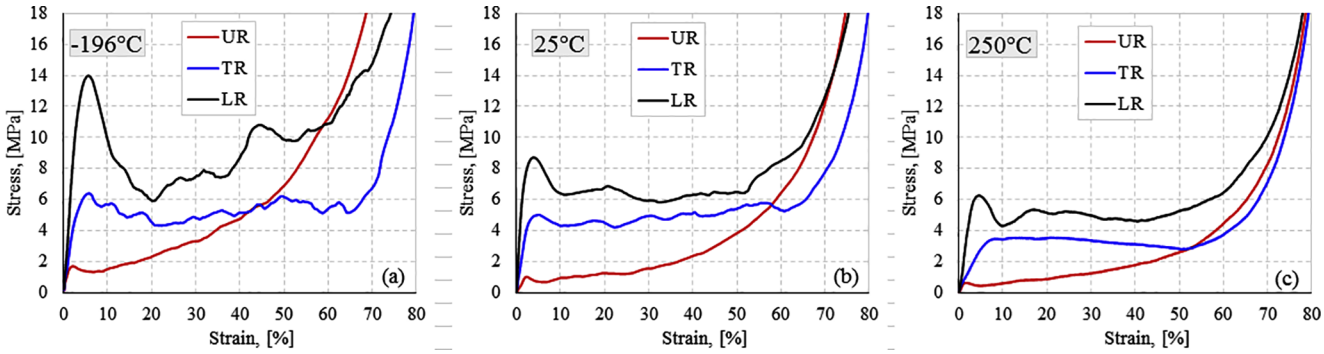

Fig. 4. Engineering stress – engineering strain curves of investigated AFs. Influence of reinforcements.

stress–strain behavior of investigated foams at average density of 0.42 g/cm^3.

Regardless of the type of reinforcements and testing temperatures, the σ-ε graphs are characterized by the typical short *linear-elastic region*, followed by a large *deformation plateau region* where the most critical failure mechanisms occur and finally a transition to *densification region* with an abrupt increase in stress at almost constant strain [50–52]. The energy absorption capacity of foams (energy absorbed per unit volume), is evaluated by integrating the area under the stress–strain curve [14,53,54]. The W increases almost linearly with strain increasing until to the onset strain of densification – OSD (see Fig. 6). The OSD and W dissipation is given by two different phenomena: the cell-walls structure collapse mechanisms and the evolution of friction between cell-walls when they are in contact.

The deformation sequences for un-/reinforced AFs together with initial (before compression tests) and final (after compression tests) shape of the foam samples at RT are presented in Fig. 7. Due to the SSFES reinforcements, from Fig. 7 it can be easily observed that the tested samples shows different deformation mechanisms.

During the experimental tests of fully dense solid materials (e.g steel, titanium etc.), one of the critical problem is the contact between the sample and the loading devices [55–59]. In the case of MFs and MFMCs, this is an insignificant problem, as any deviation of foam surfaces from parallel with regard to compressive plates are solved almost immediately by local deformations of foam. Only mirror movement or slipping is observed. If material moves, it is almost due to movement of the parts of foam with respect to the rest of foam. On the other hand, proper size of samples (diameter/size of square comparable or slightly smaller to height of sample) will also diminish significantly this problem.

The main mechanical properties of MFMCs were determined from σ-ε curves according to Ref. [49]. The following mechanical characteristics were experimentally investigated under quasi-static compressive tests: quasi-elastic modulus-E_{qe} (the slope of the compressive stress–-strain curve within the linear-elastic region), compressive yield stress-σ_y (first maximum compressive strength followed by a sudden drop in stress), strain corresponding to compressive yield stress-ε_y, $\sigma_{20\%}$ and $\sigma_{40\%}$ (compressive strength at 20% and 40% strain, respectively), plateau stress-σ_{pl} (arithmetical mean of the stresses between 20% and 40% compressive strain), densification strain-ε_D (the point in the stress–-strain curve at which the stress is 1.3 times the σ_{pl}), densification stress-σ_d (compressive strength corresponding to ε_D) and the energy absorption at densification strain-W_D. The determined properties (E_{qe}, σ_y, ε_y, σ_{pl}, σ_d, ε_d, W_D) of the investigated MFMCs samples, depending on the testing temperature, are presented in Table 1.

The total energy absorption capacity-*W*, (energy absorbed per unit volume) is defined as the amount of energy necessary to deform a given sample to specific strains and is calculated using Eq. (1) [44,60].

$$W = \int_0^{\varepsilon} \sigma d\varepsilon \tag{1}$$

The W performances of unreinforced and reinforced foams at different strains (10–80% strain with a step of 10%) and different testing temperatures are listed in Table 2.

Fig. 8 depicts the compressive properties variation with testing temperatures of AlSi10 foams with and without reinforcements.

The investigated mechanical properties (E_{qe}, σ_y, σ_{pl}, σ_d, ε_d, W) were found to be significantly smaller at higher temperature than at cryogenic temperature for both unreinforced and reinforced samples. From Fig. 8, it is obvious that the reinforced samples presents much higher properties compared to unreinforced foams at almost the same overall weight of the samples.

4. Discussions

At all investigated temperatures, the compressive σ-ε curves exhibits a yield point with an initial peak stress (σ_y) value at the end of linear-elastic region [61]. As it is obvious from Figs. 4 and 5, the highest stress drop $\Delta\sigma$ (difference between first maximum σ_y and first minimum compressive stress after σ_y) for LR foams and the lowest for TR foams

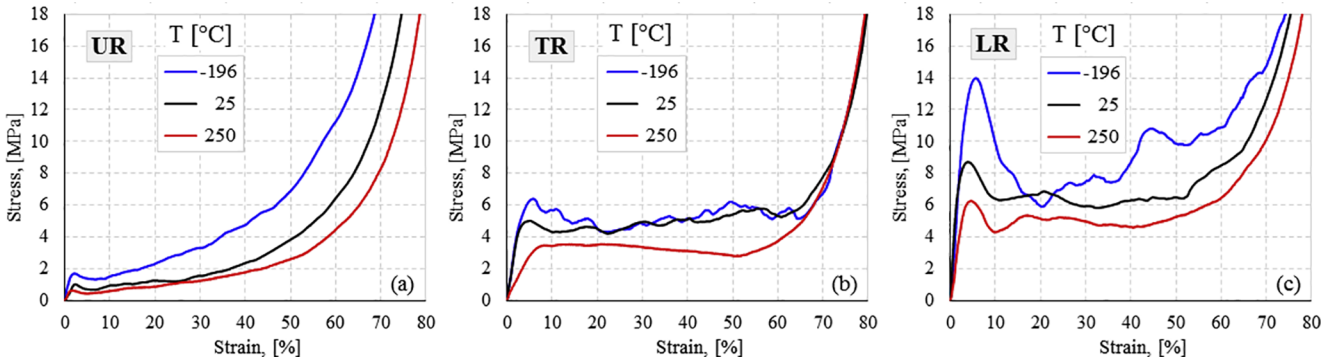

Fig. 5. Engineering stress – engineering strain curves of investigated AFs. Influence of testing temperatures.

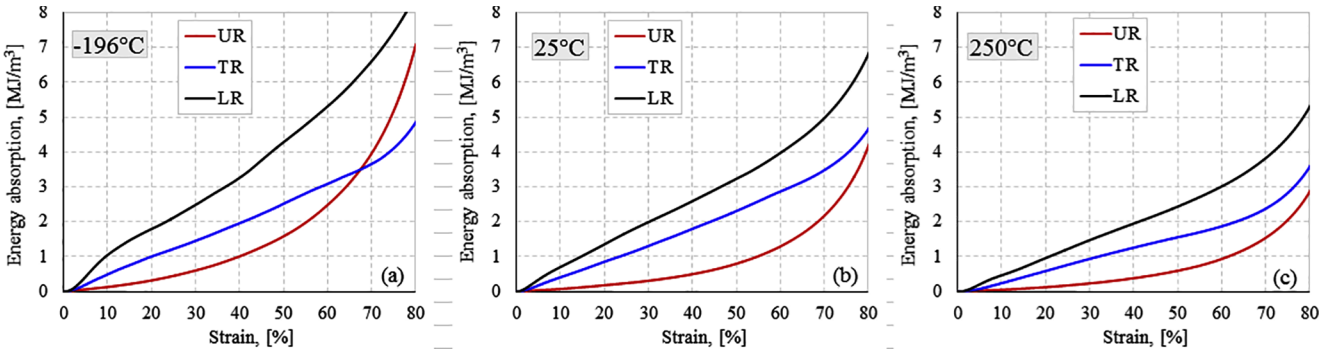

Fig. 6. Energy absorption-strain curves of investigated AFs for different testing temperatures.

was obtained. The biggest difference in Δσ terms is obtained at cryogenic temperature (i.e. 57.76% for LR, 32.45% for TR and 21.82% for UR). For reinforced foams, this difference decreases significantly with increasing test temperature (250 °C), reaching 28.01% for LR and 0.39% for TR. Otherwise, unreinforced foams show a significant increase of Δσ, of about 34.12% for 250 °C.

The plateau stress of both reinforced (TR and LR) foams highlights a pronounced serrated character after σ_y, while the absence of any stress oscillations in the case of UR foams was found [62]. The UR foams presents a continuous hardening on the entire plateau region. The serrated character of the σ-ε curves at CT and RT is mostly due to the plastic deformation of the reinforcements, together with the brittleness of the aluminum alloys used for the foam production [2,14]. Due to the morphology of the reinforcements, only a minor material separation for TR and LR foams at cryogenic temperatures was observed.

The SSFES reinforcements increases the elastic properties of the foam almost six times, though the weight due to the SSFES increases only a few percent. The biggest E_{qe} difference is obtained at HT, reducing it to 4.67% for CT. The most efficient use of SSFES reinforcement is as LR, but TR foams also show significant higher elastic properties compared to UR foams, i.e. 3.80 times (73.66%) for HT and 2.65 times (62.21%) for CT. Quasi-elastic modulus (Fig. 8a) decreases linearly with increasing test temperature.

The strength properties (σ_y, σ_{pl} and σ_d) follow the same pattern for both reinforced and unreinforced foams (see Fig. 8b–d). The strength performances of AlSi10 foams are the most beneficial influenced by the reinforcements, their properties were found considerably higher from unreinforced ones, (by 90.93% for σ_y, 65.71% for σ_{pl} and 70.89% for

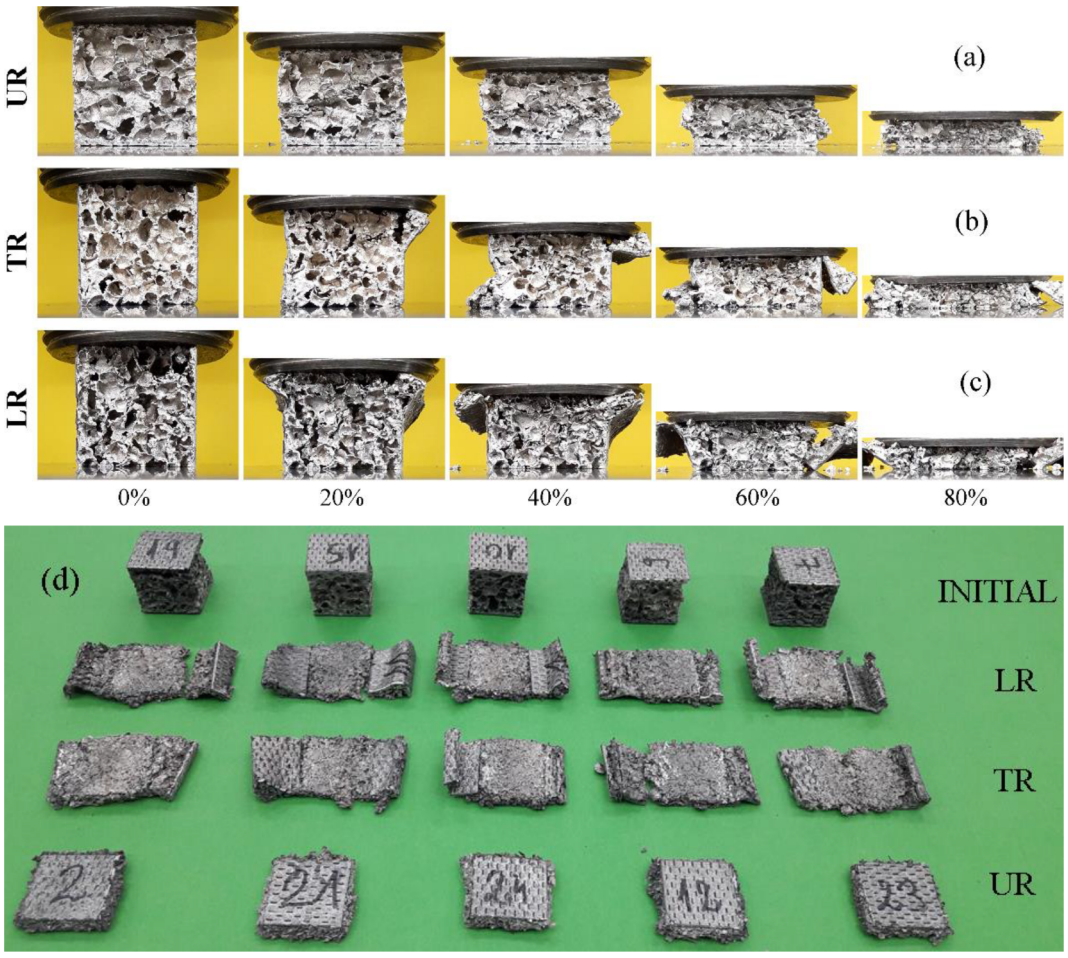

Fig. 7. RT deformation sequences (0, 20, 40, 60 and 80% strain) for UR (a), TR (b) and LR (c) foams together with initial/tested shape of the samples (d).

Table 1
The main mechanical properties of investigated AFs for different testing temperatures (average density of 0.42 g/cm^3).

Temperature [°C]	Foam type	Linear-elastic region			Plateau region			Densification region		
		E_{qe} [MPa]	σ_y [MPa]	ε_y [%]	$\sigma_{20\%}$ [MPa]	$\sigma_{40\%}$ [MPa]	σ_{pl} [MPa]	σ_D [MPa]	ε_D [%]	W_D [MJ/m^3]
−196	UR	99.51 ± 7.12	1.67 ± 0.07	2.18 ± 0.27	2.40 ± 0.17	5.19 ± 0.43	3.80 ± 0.26	4.94 ± 0.34	38.78 ± 0.42	0.98 ± 0.04
	TR	263.30 ± 20.32	7.57 ± 0.49	6.49 ± 0.52	4.47 ± 0.35	6.46 ± 0.41	5.38 ± 0.30	6.99 ± 0.61	67.33 ± 1.64	3.64 ± 0.22
	LR	464.88 ± 12.82	13.61 ± 0.38	6.29 ± 0.35	6.25 ± 0.21	7.99 ± 0.33	7.23 ± 0.11	9.40 ± 0.14	66.09 ± 1.42	5.31 ± 0.05
25	UR	61.67 ± 5.28	0.95 ± 0.11	1.95 ± 0.19	1.52 ± 0.16	2.79 ± 0.52	2.19 ± 0.21	2.56 ± 0.45	39.16 ± 0.87	0.49 ± 0.09
	TR	194.65 ± 10.34	4.69 ± 0.32	5.32 ± 0.23	4.23 ± 0.27	4.30 ± 0.44	3.97 ± 0.41	5.16 ± 0.35	65.00 ± 0.99	2.20 ± 0.16
	LR	336.00 ± 13.66	6.93 ± 0.14	3.93 ± 0.18	4.68 ± 0.20	4.33 ± 0.36	4.41 ± 0.26	6.85 ± 0.51	63.41 ± 1.03	2.95 ± 0.19
250	UR	37.38 ± 6.49	0.59 ± 0.08	1.64 ± 0.09	0.98 ± 0.42	2.09 ± 0.17	1.43 ± 0.26	1.87 ± 0.33	39.65 ± 0.52	0.41 ± 0.03
	TR	141.93 ± 16.25	3.83 ± 0.13	6.22 ± 0.38	3.54 ± 0.15	3.73 ± 0.20	3.71 ± 0.24	4.83 ± 0.27	62.75 ± 0.88	2.14 ± 0.17
	LR	220.77 ± 14.94	6.54 ± 0.28	4.85 ± 0.33	5.18 ± 0.48	4.55 ± 0.27	4.18 ± 0.32	6.41 ± 0.41	60.39 ± 0.76	2.92 ± 0.13

σ_d). Therefore, the biggest differences, up to 11.02 times (5.95 MPa), were obtained for the mechanical strength corresponding to the yield point and for HT tests. Furthermore, the compressive strength of reinforced foams depend on the orientation of the SSFES and is always higher in longitudinal direction. The expanded sheets are stronger in longitudinal direction because of larger load-bearing cross-section (see Fig. 3a, b). The strength values of LR foams are up to 40% higher than TR ones. It is important to note that the biggest drop in strength properties of reinforced foams is found between −196 °C and 25 °C (49.09% for σ_y, 39.01% for σ_{pl} and 27.09% for σ_d), while from 25 °C to 250 °C this decrease is almost insignificant (about 6%). Contrariwise, the UR foams show significant decreases in properties between both CT and RT (42.91% for σ_y, 42.20% for σ_{pl} and 48.06% for σ_d) and between RT and HT (37.76% for σ_y, 34.65% for σ_{pl} and 27.18% for σ_d).

The relatively high densification strains (67.33% strain for TR and 66.09% strain for LR) of reinforced samples at −196 °C (see Fig. 8e) is likely justified by the presence of expanded metal sheets which compensates the brittle deformation behavior of the AlSi10 matrix material. It is observed that the lack of reinforcement decreases the densification strain of UR foams up to 38.79% strain at CT. The ε_d values remain almost the same at both 25 °C and 250 °C. A slight increase (up to 39.65% strain at 250 °C) of ε_d is observed for UR foams due to the softening of the cell-walls, while the presence of reinforcements decrease slightly the ε_d values (up to 62.75% strain for TR and 60.39% strain for LR) at 250 °C. A linear variation of ε_d values with temperature for all sample configurations was obtained, Fig. 8e.

The energy absorption performances of reinforced foams are far superior to unreinforced foams, i.e. 5.45 times at CT and 7.19 times at HT. The W values of reinforced foams drops considerably from −196 °C to 25 °C (39.71% for TR and 44.51% for LR), they remain almost unchanged between 25 °C and 250 °C (decrease by only 2.73% for TR and by 0.79% for LR). Also, the LR values are up to 1.4 times higher than TR ones. As is the case of strength properties, the W values of UR foams decreases considerably between both CT-RT (49.40%) and RT-HT (17.57%).

Fig. 9 presents a comparison between reduction percentage of strength properties (yield stress, plateau stress, densification stress) and energy absorption capability at different temperatures relative to CT, for unreinforced and reinforced foam samples.

Both strength and energy-absorption reduction properties presents the same trend and are thus discussed together. The properties reduction of the reinforced foams are significantly below the reduction of the unreinforced foams. A very interesting is that even if LR foams exhibited higher mechanical properties than TR foams (see Fig. 8), TR foam reduction is much lower than that of LR foams for all investigated properties (see Fig. 9). This is due to a more stable deformation mechanism of TR foams compared to LR ones. This aspect can be easily seen from Figs. 4 and 5, where σ-ε curves show much lower oscillation amplitudes in the TR foam for all investigated temperatures, especially the plateau region.

The biggest difference between the properties reduction percentage of unreinforced and reinforced foams is observed at HT, some of them being up to 2 times smaller (plateau stress, densification stress) in the case of reinforced foams than in the case of unreinforced. Three different major effects control these property reduction differences: the mechanical properties of the foam matrix material, the deformation mechanism of the foams and the mechanical properties of reinforcements. Due to occurrence of phenomena like the dynamic recrystallization and softening of the foam matrix material at HT, the deformation behavior of the foams changes (Figs. 4 and 5) together with a significant reduction in mechanical properties (Fig. 8) [44]. At lower temperatures (−196 °C), the foams show a brittle deformation mechanism, followed by a ductile behavior at high temperature (250 °C), with a ductile-to-brittle transition around room temperature. It seems that the reinforcements take up most of the deformation mechanisms, influencing both the increase of the mechanical properties and the decrease of the percentage reduction of properties. Therefore, the mechanical properties and the correct positioning of the SSFES

Table 2
The energy absorption values of investigated AFs for different testing temperatures (average density of 0.42 g/cm^3).

T [°C]	Foam type	Energy absorption at different strains, W [MJ/m^3]							
		10%	20%	30%	40%	50%	60%	70%	80%
−196	UR	0.131 ± 0.021	0.321 ± 0.035	0.607 ± 0.061	1.012 ± 0.075	1.587 ± 0.083	2.485 ± 0.097	3.963 ± 0.180	7.068 ± 0.118
	TR	0.494 ± 0.064	1.007 ± 0.038	1.457 ± 0.028	1.961 ± 0.133	2.520 ± 0.072	3.089 ± 0.105	3.660 ± 0.101	4.850 ± 0.155
	LR	1.052 ± 0.027	1.798 ± 0.056	2.488 ± 0.053	3.264 ± 0.011	4.285 ± 0.035	5.312 ± 0.117	6.605 ± 0.234	8.537 ± 0.253
25	UR	0.073 ± 0.011	0.181 ± 0.025	0.310 ± 0.018	0.500 ± 0.066	0.801 ± 0.110	1.297 ± 0.023	2.179 ± 0.033	4.180 ± 0.228
	TR	0.411 ± 0.058	0.856 ± 0.045	1.308 ± 0.059	1.800 ± 0.074	2.310 ± 0.098	2.872 ± 0.082	3.486 ± 0.171	4.665 ± 0.0271
	LR	0.707 ± 0.013	1.356 ± 0.040	1.992 ± 0.037	2.595 ± 0.102	3.234 ± 0.083	3.977 ± 0.118	4.978 ± 0.294	6.820 ± 0.319
250	UR	0.049 ± 0.005	0.126 ± 0.038	0.233 ± 0.026	0.384 ± 0.041	0.599 ± 0.009	0.937 ± 0.056	1.544 ± 0.040	2.868 ± 0.083
	TR	0.242 ± 0.082	0.591 ± 0.073	0.938 ± 0.055	1.260 ± 0.037	1.558 ± 0.078	1.871 ± 0.029	2.379 ± 0.077	3.585 ± 0.194
	LR	0.468 ± 0.041	0.965 ± 0.063	1.476 ± 0.095	1.952 ± 0.084	2.439 ± 0.064	3.016 ± 0.145	3.830 ± 0.123	5.301 ± 0.228

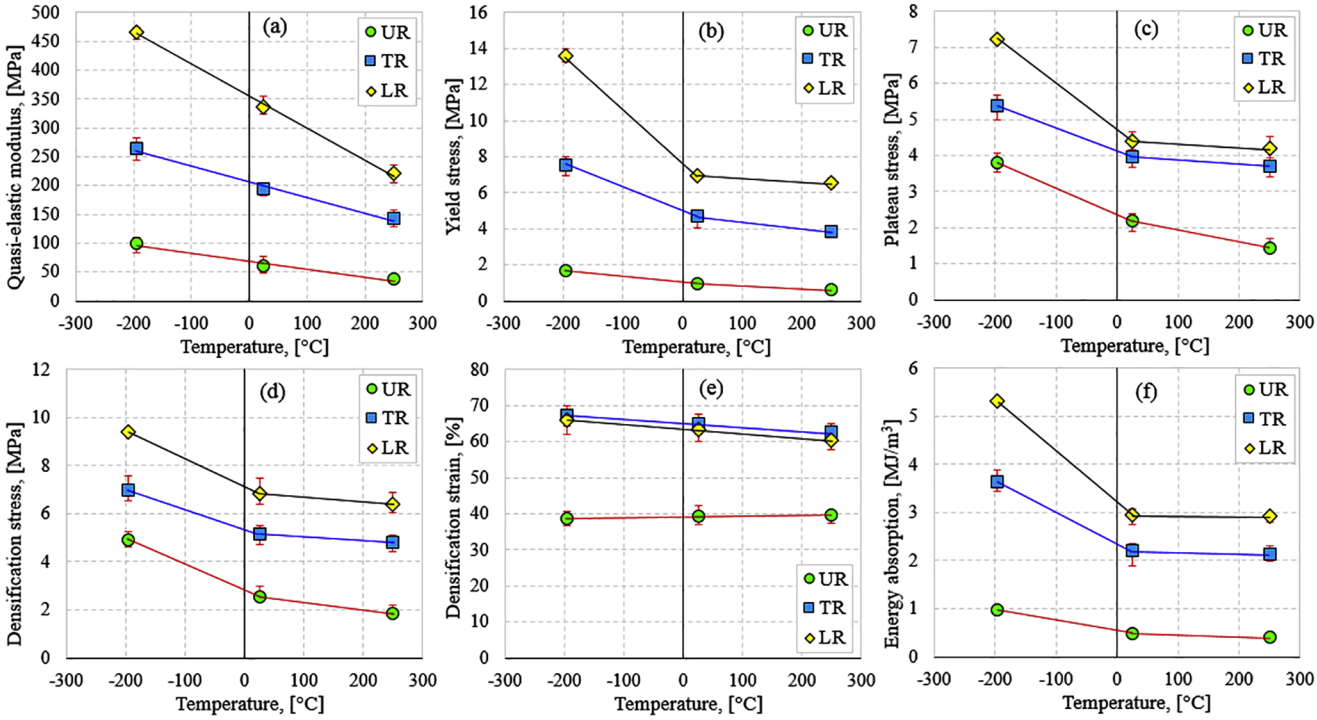

Fig. 8. Variation of investigated AFs mechanical properties with testing temperature.

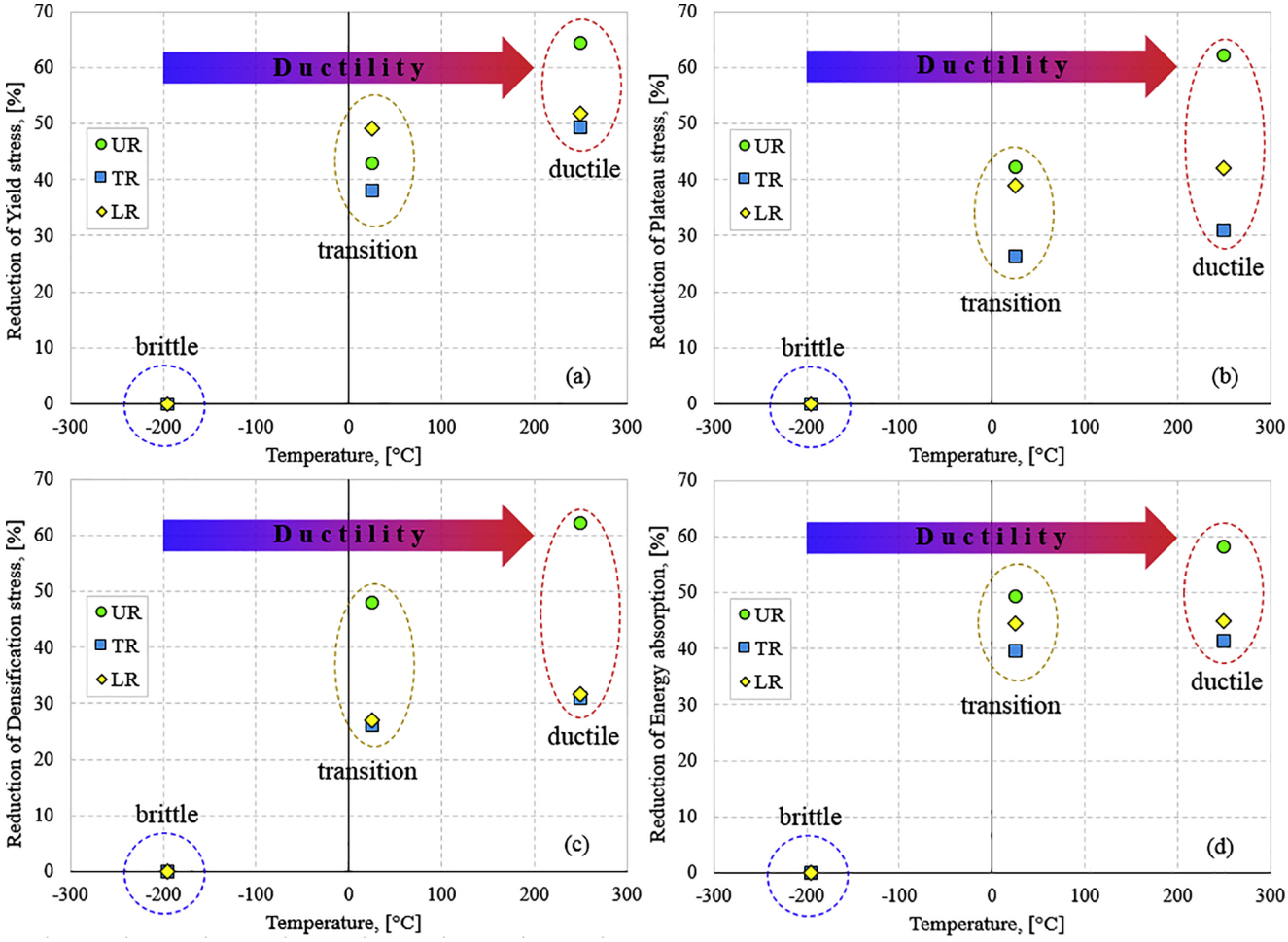

Fig. 9. Reduction percentage of AFs mechanical properties at different temperatures normalized by CT value.

reinforcements become the dominant deformation mechanism.

Future development can be in replacing complex 3D castings of aluminum with 3D complex parts made from aluminum foam reinforced in proper directions with stainless steel mesh. The obtained results can be employed in numerical calculations to obtain proper size, placement and orientation of stainless steel mesh to obtain enough stiff and strength goods at minimum weight. Future works can be in varying strain rate at the investigated temperatures.

5. Conclusions

Quasi-static compressive mechanical properties (quasi-elastic modulus, yield stress, plateau stress, densification stress, densification strain and energy absorption capacity) of high porosity reinforced closed-cell aluminum alloy foams subjected to cryogenic (−196 °C using liquid nitrogen) and high (250 °C using a thermal chamber) temperatures has been investigated at average density of 0.42 g/cm^3. The following conclusions can be drawn:

The behavior and mechanical properties of reinforced foam samples are a function of the positioning of the reinforcement cells according to the loading direction. The experimental tests showed that, the reinforcements affects the magnitude of the compressive plateau stress. Thus, the foam samples with longitudinal reinforcements (LR) exhibit high-energy absorption capacity because of the high compressive strength.

The strength properties and energy absorption performances of investigated foams are the highest at the cryogenic temperature and similarly decrease with increasing test temperature. Moreover, the foam deformation mechanism changes (due to the dynamic recrystallization and softening of the foam matrix material) from brittle (−196 °C) to ductile (250 °C) around the 25 °C transition temperature.

The percentage reductions of the reinforced foams are significantly below the reduction of the unreinforced foam. Furthermore, the transversal reinforced (TR) foam reduction is lower than that of LR foams, even if LR foams exhibited higher properties than TR foams.

Conclusively, the foam mechanical properties (E_{qe}, σ_y, σ_{pl}, σ_d, ε_d, W) at all investigated temperatures (−196, 25, 250 °C) are substantially improved by using expanded metal reinforcements for at almost the same overall weight of the samples. The data resulted from the experimental program given in this work can further be used in the design phase of a cryogenic storage or fuel tanks application.

Acknowledgement

This work was partially supported by research grants PCD-TC-2017 and PN-III-P1-1.2-PCCDI-2017-0391/CIA_CLIM.

References

[1] Ashby MF, Evans A, Fleck NA, et al. Metal foams: a design guide. USA: Butterworth-Heinemann; 2000.
[2] Marsavina L, Kovacik J, Linul E. Experimental validation of micromechanical models for brittle aluminium alloy foam. Theor Appl Fract Mech 2016;83:11–8.
[3] Ciardiello R, Drzal LT, Belingardi G. Effects of carbon black and graphene nanoplatelet fillers on the mechanical properties of syntactic foam. Compos Struct 2017;178:9–19.
[4] Marx J, Portanova M, Rabiei A. A study on blast and fragment resistance of composite metal foams through experimental and modeling approaches. Compos Struct 2018;194:652–61.
[5] Katona B, Szlancsik A, Tábi T, Orbulov IN. Compressive characteristics and low frequency damping of aluminium matrix syntactic foams. Mat Sci Eng A 2019;739:140–8.
[6] Kádár C, Máthis K, Orbulov IN, Chmelík F. Monitoring the failure mechanisms in metal matrix syntactic foams during compression by acoustic emission. Mater Lett 2015;173:31–4.
[7] Taherishargh M, Linul E, Broxtermann S, Fiedler T. The mechanical properties of expanded perlite-aluminium syntactic foam at elevated temperatures. J Alloy Compd 2018;737:590–6.
[8] Katona B, Szebényi G, Orbulov IN. Fatigue properties of ceramic hollow sphere filled aluminium matrix syntactic foams. Mat Sci Eng A 2017;679:350–7.
[9] Luong D, Shunmugasamy V, Gupta N, Lehmhus D, et al. Quasi-static and high strain rates compressive response of iron and Invar matrix syntactic foams. Mater Des 2015;66:516–31.
[10] An Y, Yang S, Zhao E, Wang Z. Characterization of metal grid-structure reinforced aluminum foam under quasi-static bending loads. Compos Struct 2017;178:288–96.
[11] Linul E, Şerban DA, Marsavina L, Kovacik J. Low-cycle fatigue behaviour of ductile closed-cell aluminium alloy foams. Fatig Fract Eng Mater Struct 2017;40(4):597–604.
[12] Liu C, Zhang YX, Li J. Impact responses of sandwich panels with fibre metal laminate skins and aluminium foam core. Compos Struct 2017;182:183–90.
[13] Sun G, Li S, Liu Q, Li G, Li Q. Experimental study on crashworthiness of empty/aluminum foam/honeycomb-filled CFRP tubes. Compos Struct 2016;152:969–93.
[14] Linul E, Movahedi N, Marsavina L. The temperature effect on the quasi-static compressive behavior of ex-situ aluminum foam-filled tubes. Compos Struct 2017;180:709–22.
[15] Liang M, Lu F, Zhang G, Li X. Experimental and numerical study of aluminum foam-cored sandwich tubes subjected to internal air blast. Compos Part B 2017;125:134–43.
[16] Liu Z, Huang Z, Qin Q. Experimental and theoretical investigations on lateral crushing of aluminum foam-filled circular tubes. Compos Struct 2017;175:19–27.
[17] Al-Sahlani K, Broxtermann S, Lell D, Fiedler T. Effects of particle size on the microstructure and mechanical properties of expanded glass-metal syntactic foams. Mat Sci Eng A 2018;728:80–7.
[18] Linul E, Serban DA, Marsavina L. Influence of cell topology on mode I fracture toughness of cellular structures. Phys Mesomech 2018;21(2):178–86.
[19] Kovácik J, Jerz J, Mináriková N, et al. Scaling of compression strength in disordered solids: metallic foams. Frattura ed Integrità Strutturale 2016;36:55–62.
[20] Jurgens RF. High-temperature electronics applications in space exploration. NASA Lewis Res Center Proc Conf. High-Temp. Electron 1981:3–7.
[21] Patterson RL, Hammoud A, Elbuluk M. Assessment of electronics for cryogenic space exploration missions. Cryogenics 2006;46:231–6.
[22] Linul E, Marsavina L, Kovacik J, Sadowski T. Dynamic and quasi-static compression tests of closed-cell aluminium alloy foams. P Romanian Acad A 2017;18(4):361–9.
[23] Taherishargh M, Belova IV, Murch GE, Fiedler T. The effect of particle shape on mechanical properties of perlite/metal syntactic foam. J Alloy Compd 2017;693:55–60.
[24] Liu Q, Fu J, Wang J, et al. Axial and lateral crushing responses of aluminum honeycombs filled with EPP foam. Compos Part B 2017;130:236–47.
[25] Shahapurkar K, Garcia CD, Doddamani M, et al. Compressive behavior of cenosphere/epoxy syntactic foams in arctic conditions. Compos Part B 2018;135:253–62.
[26] Movahedi N, Linul E. Mechanical properties of light expanded clay aggregated (LECA) filled tubes. Mater Lett 2018;217:194–7.
[27] Wang L, Fan X, Chen H, Liu W. Axial crush behavior and energy absorption capability of foam-filled GFRP tubes under elevated and high temperatures. Compos Struct 2016;149:339–50.
[28] Li Z, Chen X, Jiang B, Lu F. Local indentation of aluminum foam core sandwich beams at elevated temperatures. Compos Struct 2016;145:142–8.
[29] Linul E, Şerban DA, Marsavina L, Sadowski T. Assessment of collapse diagrams of rigid polyurethane foams under dynamic loading conditions. Arch Civ Mech Eng 2017;17(3):457–66.
[30] Linul L, Movahedi N, Marsavina L. On the lateral compressive behavior of empty and ex-situ aluminum foam-filled tubes at high temperature. Materials 2018;11(4):554.
[31] Yu YH, Choi I, Nam S, Lee DG. Cryogenic characteristics of chopped glass fiber reinforced polyurethane foam. Compos Struct 2014;107:476–81.
[32] Yu YH, Nam S, Lee D, Lee DG. Cryogenic impact resistance of chopped fiber reinforced polyurethane foam. Compos Struct 2015;132:12–9.
[33] Park SB, Lee CS, Choi SW, et al. Polymeric foams for cryogenic temperature application: temperature range for non-recovery and brittle-fracture of microstructure. Compos Struct 2016;136:258–69.
[34] Choi I, Yu YH, Lee DG. Cryogenic sandwich-type insulation board composed of E-glass/epoxy composite and polymeric foams. Compos Struct 2013;102:61–71.
[35] Fesmire JE, Coffman BE, Meneghelli BJ, Heckle KW. Spray-on foam insulations for launch vehicle cryogenic tanks. Cryogenics 2012;52:251–61.
[36] Dixit T, Ghosh I. Radiation heat transfer in high porosity open-cell metal foams for cryogenic applications. Appl Therm Eng 2016;102:942–51.
[37] Dixit T, Ghosh I. Cooling capacity of high porosity open-cell metal foams as passive cryogenic radiators. Cryogenics 2017;84:81–8.
[38] Chunhui K, Liubiao C, Xianlin W, et al. Thermal conductivity of open cell aluminum foam and its application as advanced thermal storage unit at low temperature. Rare Metal Mat Eng 2018;47(4):1049–53.
[39] Dimassia MA, John M, Herrmann AS. Investigation of the temperature dependent impact behaviour of pin reinforced foam core sandwich structures. Compos Struct 2018;202:774–82.
[40] Park SB, Choi SW, Kim JH, et al. Effect of the blowing agent on the low-temperature mechanical properties of CO2- and HFC-245fa-blown glass-fiber-reinforced polyurethane foams. Compos Part B 2016;93:317–27.
[41] Zhang XB, Yao L, Qiu LM, et al. Experimental study on cryogenic moisture uptake in polyurethane foam insulation material. Cryogenics 2012;52:810–5.
[42] Kim TR, Shin JK, Goh TS, et al. Modeling of elasto-viscoplastic behavior for polyurethane foam under various strain rates and temperatures. Compos Struct 2017;180:686–95.
[43] Russo P, Langella A, Papa I. Thermoplastic polyurethane/glass fabric composite laminates: low velocity impact behavior under extreme temperature conditions. Compos Struct 2017;166:146–52.
[44] Movahedi N, Linul E, Marsavina L. The temperature effect on the compressive

behavior of closed-cell aluminum-alloy foams. J Mater Eng Perform 2018;27(1):99–108.
[45] Xi H, Tang L, Luo S, et al. A numerical study of temperature effect on the penetration of aluminum foam sandwich panels under impact. Compos Part B 2017;130:217–29.
[46] Broxtermann S, Taherishargh M, Belova IV, et al. On the compressive behaviour of high porosity expanded Perlite-Metal Syntactic Foam (P-MSF). J Alloy Compd 2017;691:690–7.
[47] Linul E, Marsavina L, Kováčik J. Collapse mechanisms of metal foam matrix composites under static and dynamic loading conditions. Mat Sci Eng A 2017;690:214–24.
[48] Simancik F, Rajner W, Laag R. Reinforced Alulight for structural use. In: Processing and properties of Lightweight Cellular Metals and Structures (TMS Annual Meeting), Seattle, 2002. p. 25.
[49] ISO 13314. Mechanical testing of metals – Ductility testing – Compression test for porous and cellular metals. 2011.
[50] Fiedler T, Taherishargh M, Krstulović-Opara L, Vesenjak M. Dynamic compressive loading of expanded perlite/aluminum syntactic foam. Mat Sci Eng A 2015;626:296–304.
[51] Movahedi N, Linul E. Quasi-static compressive behavior of the ex-situ aluminum-alloy foam-filled tubes under elevated temperature conditions. Mater Lett 2017;206:182–4.
[52] Pang X, Du H. Dynamic characteristics of aluminium foams under impact crushing. Compos Part B 2017;112:265–77.
[53] Broxtermann S, Vesenjak M, Krstulović-Opara L, Fiedler T. Quasi static and dynamic compression of zinc syntactic foams. J Alloy Compd 2018;768:962–9.
[54] Kovacik J, Marsavina L, Linul E. Poisson's ratio of closed-cell aluminium foams. Materials 2018;11(10):1904.
[55] Zhou XP, Lian YJ, Wong LNY, Berto F. Understanding the fracture behavior of brittle and ductile multiflawed rocks by uniaxial loading by digital image correlation. Eng Fract Mech 2018;199:438–60.
[56] Derpeński Ł, Seweryn A, Berto F. Brittle fracture of axisymmetric specimens with notches made of graphite EG0022A. Theor Appl Fract Mech 2017;89:45–51.
[57] Razavi SMJ, Ayatollahi MR, Majidi HR, Berto F. A strain-based criterion for failure load prediction of steel/CFRP double strap joints. Compos Struct 2018;206:116–23.
[58] Peron M, Torgersen J, Berto F. Rupture predictions of notched Ti-6Al-4V using local approaches. Materials 2018;11(5):663.
[59] Ferro P, Bonollo F, Bassan F, Berto F. Strain evolution in cold-warm forged steel components studied by means of EBSD technique. Materials 2017;10(12):1441.
[60] Rajak DK, Mahajan NN, Linul E. Crashworthiness performance and microstructural characteristics of foam-filled thin-walled tubes under diverse strain rate. J Alloy Compd 2019;775:675–89.
[61] Ghiani C, Linul E, Porcu MC, et al. Metal foam-filled tubes as plastic dissipaters in earthquake-resistant steel buildings. IOP Conf Ser: Mater Sci Eng 2018;416:012051.
[62] Linul E, Marsavina L, Kovacik J. Compressive behavior and energy absorption capability of reinforced closed-cell aluminum alloy foams. IOP Conf Ser: Mater Sci Eng 2018;416:012079.